Radiology

Release of Cell-free MicroRNA Tumor Biomarkers into the Blood Circulation with Pulsed Focused Ultrasound: A Noninvasive, Anatomically Localized, Molecular Liquid Biopsy[1]

John R. Chevillet, PhD
Tatiana D. Khokhlova, PhD
Maria D. Giraldez, MD, PhD
George R. Schade, MD
Frank Starr, BS
Yak-Nam Wang, PhD
Emily N. Gallichotte, BA
Kai Wang, PhD
Joo Ha Hwang, MD, PhD
Muneesh Tewari, MD, PhD

Purpose: To compare the abilities of three pulsed focused ultrasound regimes (that cause tissue liquefaction, permeabilization, or mild heating) to release tumor-derived microRNA into the circulation in vivo and to evaluate release dynamics.

Materials and Methods: All rat experiments were approved by the University of Washington Institutional Animal Care and Use Committee. Reverse-transcription quantitative polymerase chain reaction array profiling was used to identify candidate microRNA biomarkers in a rat solid tumor cell line. Rats subcutaneously grafted with these cells were randomly assigned among three pulsed focused ultrasound treatment groups: *(a)* local tissue liquefaction via boiling histotripsy, *(b)* tissue permeabilization via inertial cavitation, and *(c)* mild (<10°C) heating of tissue, as well as a sham-treated control group. Blood specimens were drawn immediately prior to treatment and serially over 24 hours afterward. Plasma microRNA was quantified with reverse-transcription quantitative polymerase chain reaction, and statistical significance was determined with one-way analysis of variance (Kruskal-Wallis and Friedman tests), followed by the Dunn multiple-comparisons test.

Results: After tissue liquefaction and cavitation treatments (but not mild heating), plasma quantities of candidate biomarkers increased significantly (P value range, <.0001 to .04) relative to sham-treated controls. A threefold to 32-fold increase occurred within 15 minutes after initiation of pulsed focused ultrasound tumor treatment, and these increases persisted for 3 hours. Histologic examination confirmed complete liquefaction of the targeted tumor area with boiling histotripsy, in addition to areas of petechial hemorrhage and tissue disruption by means of cavitation-based treatment.

Conclusion: Mechanical tumor tissue disruption with pulsed focused ultrasound–induced bubble activity significantly increases the plasma abundance of tumor-derived microRNA rapidly after treatment.

Online supplemental material is available for this article.

[1] From the Division of Human Biology, Fred Hutchinson Cancer Research Center, Seattle, Wash (J.R.C., E.N.G., M.D.G., M.T.); Institute for Systems Biology, Seattle, Wash (J.R.C., K.W.); Department of Medicine (T.D.K., J.H.H.), Department of Urology (G.R.S.), and Applied Physics Laboratory (F.S., Y.N.W.), University of Washington, Seattle, Wash; and Departments of Internal Medicine (M.D.G., M.T.) and Biomedical Engineering, Center for Computational Medicine and Bioinformatics, and the Biointerfaces Institute (M.T.), University of Michigan, 109 Zina Pitcher Pl, 1502 BSRB, SPC 2200, Ann Arbor, MI 48109. Received January 6, 2016; revision requested March 25; revision received June 21; accepted July 28; final version accepted August 26. **Address correspondence to** M.T. (e-mail: *mtewari@med.umich.edu*).

J.R.C. supported by a Canary Foundation and American Cancer Society Postdoctoral Fellowship for the Early Detection of Cancer (PFTED-09-249-01-SEID), the Hillcrest Committee of Southern Oregon, and the Center for Systems Biology of the National Institutes of Health (NIH) (P50GM076547). T.D.K. supported by the NIH Career Development Award (K01EB015745-01). M.D.G. supported by Rio Hortega and Martin Escudero Fellowships. Y.N.W. supported by the NIH (R01EB7643). K.W. supported by the Center for Systems Biology of the NIH (P50GM076547). M.T. supported by the NIH Transformative R01 grant (R01DK085714), the Stand Up To Cancer Innovative Research Grant (SU2C-AACR-IRG1109), a Damon Runyon-Rachleff Innovation Award, a Prostate Cancer Foundation Creativity Award, and support from the Canary Foundation.

J.R.C. and T.D.K. contributed equally to this work.

An essential element of precision medicine in oncology is the ability to observe and quantify molecular alterations that serve as biomarkers (eg, gene expression signatures and somatic mutations) (1,2). Biomarker analysis typically requires tissue biopsy, which is invasive, may involve inadequate sampling of heterogeneous tumors, and can be associated with patient discomfort and risk for complications (3–8). Tissue biopsy is also not routinely feasible for longitudinal measurement of biomarkers in patients undergoing treatment. In light of these limitations, blood-based, cell-free circulating nucleic acids (eg, plasma and serum microRNA [miRNA] and DNA) are being developed as biomarkers (9–11). This approach would enable repeatable, minimally invasive tumor diagnosis and monitoring. However, two key challenges with this use of circulating nucleic acids are *(a)* low quantities in blood (especially in early-stage disease) (12,13) and *(b)* no identification of anatomic origin (ie, tumor location). Thus, a minimally invasive method to stimulate nucleic acid biomarker release from a specific site of interest into the circulation would be clinically useful.

In an independent study (14), investigators reported that unfocused, low-intensity ultrasound treatment of a tumor significantly ($P = .03$) increased the plasma concentration of the cell surface and secreted glycoprotein biomarker carcinoembryonic antigen (CEA) in a murine model. Although unclear, the most likely cause of CEA shedding is mild, sublethal soft-tissue heating (15). However, it is uncertain whether such exposures could release intracellular molecules (eg, RNA and DNA). Here, we considered ultrasound-based approaches with the ability to disrupt cellular membrane integrity to release such molecules into the extracellular space and, ultimately, the circulation.

Pulsed focused ultrasound allows induction of such mechanical tissue disruption locally and noninvasively, while minimizing off-target effects (16). With pulsed focused ultrasound, short bursts of high-amplitude ultrasound waves are used from an extracorporeal source. These induce transient bubble activity at the defined anatomic focus. Mechanical damage to tissue can be controlled by choosing a pulsed focused ultrasound treatment protocol, ranging from scattered, micron-sized disruption to millimeter-sized regions of complete tissue liquefaction. The former approach has been well established in pulsed focused ultrasound–aided drug and gene delivery applications, with and without ultrasonographic (US) contrast agents (17–19). The latter is collectively referred to as histotripsy. In one implementation, termed *boiling histotripsy* (BH), a highly nonlinear ultrasound pulse rapidly (in milliseconds) superheats the focal point and induces a vapor bubble (20,21). The interaction of the bubble and the remaining ultrasound pulse lyses cells without detectable thermal injury (Fig 1).

The purpose of this study was to compare the abilities of three pulsed focused ultrasound regimes (that cause tissue liquefaction, permeabilization, or mild heating) to release tumor-derived miRNA into the circulation in vivo and to evaluate release dynamics.

Advances in Knowledge

- Mechanical disruption of tumor tissue by pulsed focused ultrasound–induced bubble activity increases the abundance of candidate microRNA tumor biomarkers in the blood circulation of a rodent model by threefold to 32-fold.
- Significant microRNA release ($P = .01–.02$) occurs within 2 minutes of pulsed focused ultrasound initiation, consistent with acute release from target cells due to disruption of cell membrane integrity.
- Both boiling histotripsy and cavitation-based tissue permeabilization increased circulating microRNA quantities, which indicates that complete tissue liquefaction is not required and micron-sized tissue disruption is sufficient to release nucleic acids from tumors.

Implications for Patient Care

- Pulsed focused ultrasound provides a means to stimulate the release of tumor-associated microRNA from a specific anatomic tumor site into the circulation in a preclinical model.
- Pulsed focused ultrasound amplification of circulating nucleic acid cancer biomarkers may provide clinical utility for the diagnosis and molecular phenotyping of early disease and/or allow for serial "liquid biopsy" over the course of cancer therapy to monitor treatment response and tumor evolution.

Materials and Methods

J.R.C., T.D.K., G.R.S., J.H.H., and M.T. are coauthors on a patent application regarding noninvasive biopsy by using high-intensity focused ultrasound. T.D.K. and J.H.H. are coauthors on patent applications regarding noninvasive treatment of tissue by using high-intensity focused ultrasound and imaging bubbles in a medium.

Published online before print
10.1148/radiol.2016160024 **Content code:** US

Radiology 2017; 283:158–167

Abbreviations:
BH = boiling histotripsy
CEA = carcinoembryonic antigen
miRNA = microRNA
qPCR = quantitative polymerase chain reaction
RT = reverse-transcription

Author contributions:
Guarantors of integrity of entire study, J.R.C., E.N.G., M.T.; study concepts/study design or data acquisition or data analysis/interpretation, all authors; manuscript drafting or manuscript revision for important intellectual content, all authors; approval of final version of submitted manuscript, all authors; agrees to ensure any questions related to the work are appropriately resolved, all authors; literature research, J.R.C., T.D.K., M.D.G., G.R.S., M.T.; experimental studies, J.R.C., T.D.K., M.D.G., G.R.S., F.S., Y.N.W., E.N.G., K.W.; statistical analysis, J.R.C., T.D.K., M.D.G., G.R.S.; and manuscript editing, J.R.C., T.D.K., M.D.G., G.R.S., Y.N.W., E.N.G., M.T.

Conflicts of interest are listed at the end of this article.

Rodent Model

All rat experiments were performed by individuals with experience in tumor implantation (T.D.K. and F.S., with 6 and 20 years of experience, respectively) and pulsed focused ultrasound treatment (T.D.K., with 6 years of experience) and in accordance with University of Washington Institutional Animal Care and Use Committee–approved protocols. Intact adult male Copenhagen rats 7–9 weeks of age were surgically implanted with jugular vein polyurethane catheters (Charles River Laboratories, Wilmington, Mass) for repeated blood sampling. Rats were then subcutaneously grafted with 5×10^5 syngeneic MatLyLu cells (22), and the tumors were allowed to grow to 1 cm in diameter over 9–11 days before pulsed focused ultrasound treatment was applied.

Focused Ultrasound Treatment System

A customized VIFU 2000 preclinical focused ultrasound system (Alpinion Medical Systems, Bothell, Wash) was used in all experiments (Fig 2a). A 1.5-MHz single-element, spherically focused transducer (64-mm aperture

Figure 1

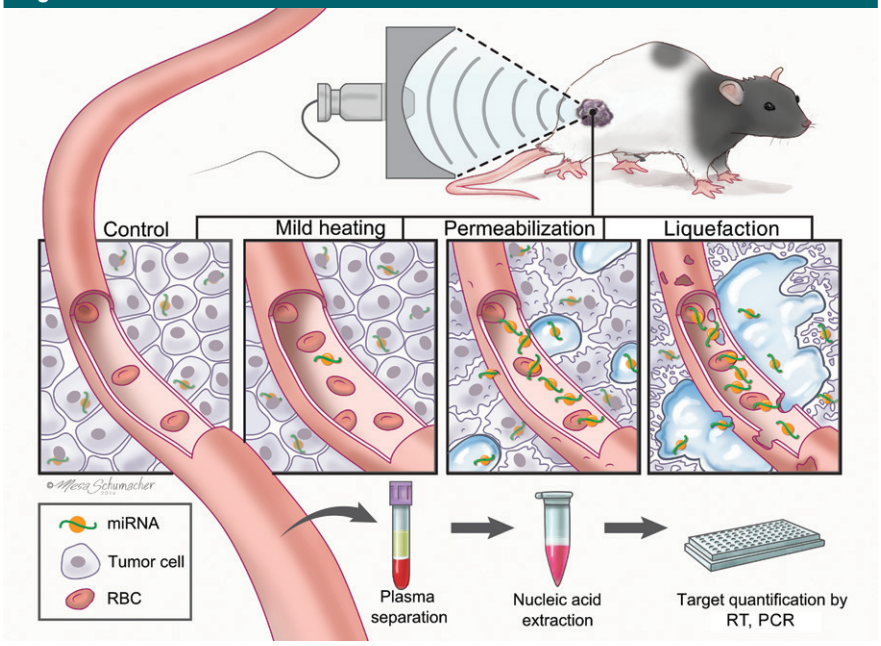

Figure 1: Illustration of the study design and hypothesis, involving mechanisms of pulsed focused ultrasound–induced release of tumor-derived miRNAs. At lower intensities, focused ultrasound can produce mild, sublethal heating of tissue, thus potentially causing additional release of miRNAs through increased circulation and vasodilation. High-amplitude, pulsed regimes of focused ultrasound that promote bubble activity in tissue can cause permeabilization of cell membranes and vessel walls or complete liquefaction of the localized areas of tissue. These regimes have the potential to directly release the intracellular miRNAs into the circulation, where they can be detected in a blood sample. *qPCR* = quantitative polymerase chain reaction, *RBC* = red blood cell, *RT* = *reverse-transcription*.

Figure 2

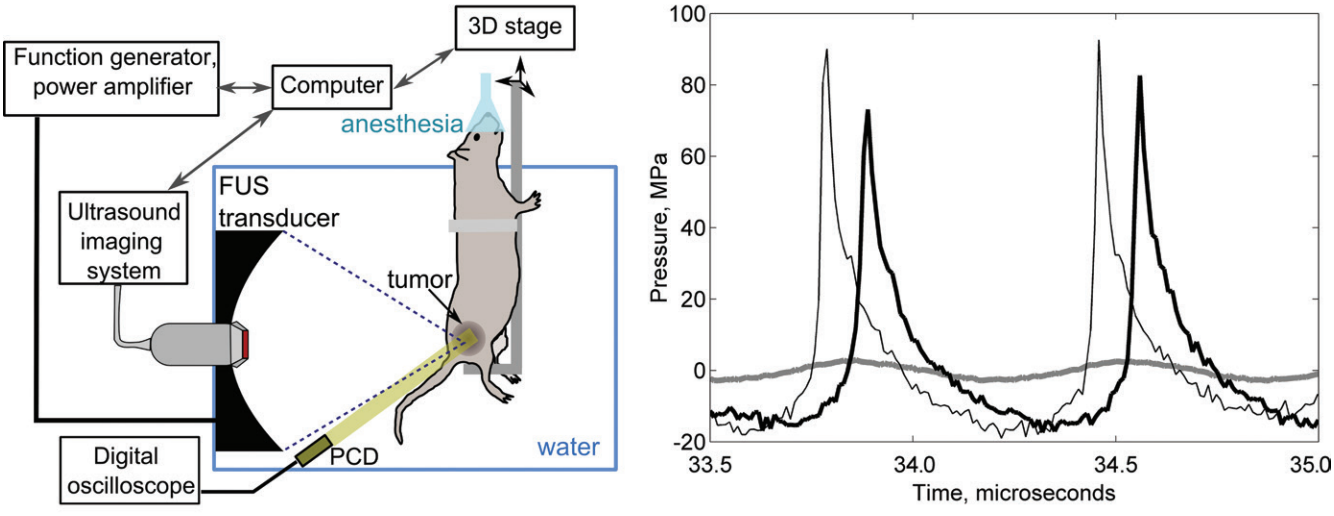

a. b.

Figure 2: **(a)** Schematic diagram of the experimental setup. **(b)** Graph shows the focal pulsed ultrasound pressure waveforms used for the three treatment regimes: tissue liquefaction (thin black line), tissue permeabilization (thick black line), and mild heating (thick gray line) as measured in water by using a fiber-optic probe hydrophone. Peak US pressures and details of pulsing protocols for each treatment regimen are summarized in Table 1. *FUS* = focused ultrasound, *PCD* = passive cavitation detector, *3D* = three-dimensional.

and 45-mm radius of curvature) was mounted in an acrylic water tank and powered by a computer-controlled function generator and power amplifier. The electrical power available to the focused ultrasound transducer could be varied within a 25–600-W range. The focused ultrasound transducer had a circular central opening, fitted with a US imaging probe (C4-12 phased-array probe with center frequency of 7 MHz) for treatment planning and monitoring. The ultrasound focus location was preregistered with the imaging system and indicated on the monitor by a white cross (Fig 3) for convenient, in-line targeting of the tumor. A custom-built animal holder was attached to the computer-controlled three-dimensional positioning system and immersed in the water tank equipped with a water conditioning system for continuous degassing, heating, and filtering.

The focal pressure waveforms produced by the pulsed focused ultrasound transducer at different power levels were measured in the water by using the fiber-optic probe hydrophone (FOPH2000; RP Acoustics, Leutenbach, Germany). The focal pressure waveforms that corresponded to the three pulsed focused ultrasound treatment types used in our study (tissue liquefaction, permeabilization, and mild heating) are shown in Figure 2b, and the peak focal pressures are summarized in the Table.

Ultrasound Treatment and Blood Collection

Animals were randomly divided into four groups, which corresponded to the three different types of pulsed focused ultrasound treatment: tissue liquefaction via BH (n = 9), tissue permeabilization via inertial cavitation (n = 6), and mild tissue heating (n = 9), as well as a sham control group (n = 9). The details of each pulsed focused ultrasound treatment type are summarized below. Each animal was anesthetized by means of isoflurane inhalation, and the tumor site was shaved and depilated. High-resolution US imaging was performed (L8-17 probe with a center frequency of 12 MHz) to precisely measure the tumor dimensions. After a pretreatment blood draw, the animal was positioned in the holder, and the target area was submerged into the 37°C water tank for treatment planning.

Treatment planning was performed with B-mode US image guidance. The ultrasound focus (the white cross on the US image in Fig 3) was aligned with the center of the tumor in the axial plane. The focused ultrasound treatment grid in the two transverse dimensions was then generated to cover most of the tumor region. Treatment spots were separated by 2 mm. Shallow regions of the tumor were intentionally left untreated to avoid potential skin damage. During treatment, the animal holder was moved in a raster pattern to position the ultrasound focus at each of the planned treatment spots. During tissue liquefaction via BH, the hyperechoic

Figure 3

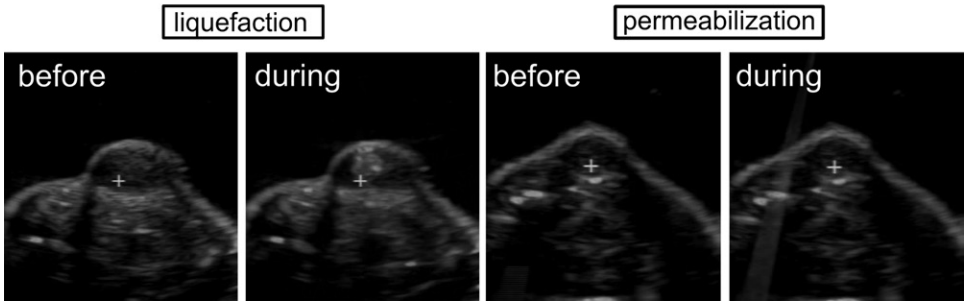

Figure 3: US B-mode images of the tumor obtained before and during tissue liquefaction with pulsed focused ultrasound (left) or before and during permeabilization with pulsed focused ultrasound (right). The white cross indicates the position of the ultrasound focus during treatment; pulsed focused ultrasound is incident from the top of the images. A hyperechoic region that corresponds to a large bubble appears prefocally during liquefaction treatment and allows monitoring of treatment progression. No changes to the B-mode images of the tumor are observed during permeabilization treatment.

Characteristics of the Pulsed Focused Ultrasound Regimes Used in the Study

Treatment Type	Peak Compressional Focal Pressure (MPa)	Peak Rarefactional Focal Pressure (MPa)	Pulse Duration (msec)	Pulse Repetition Frequency (Hz)	Time per Spot (sec)
Liquefaction	90	17	10	1	30
Permeabilization	78	16	1	1	30
Mild heating	2.5	2.3	2	250	30

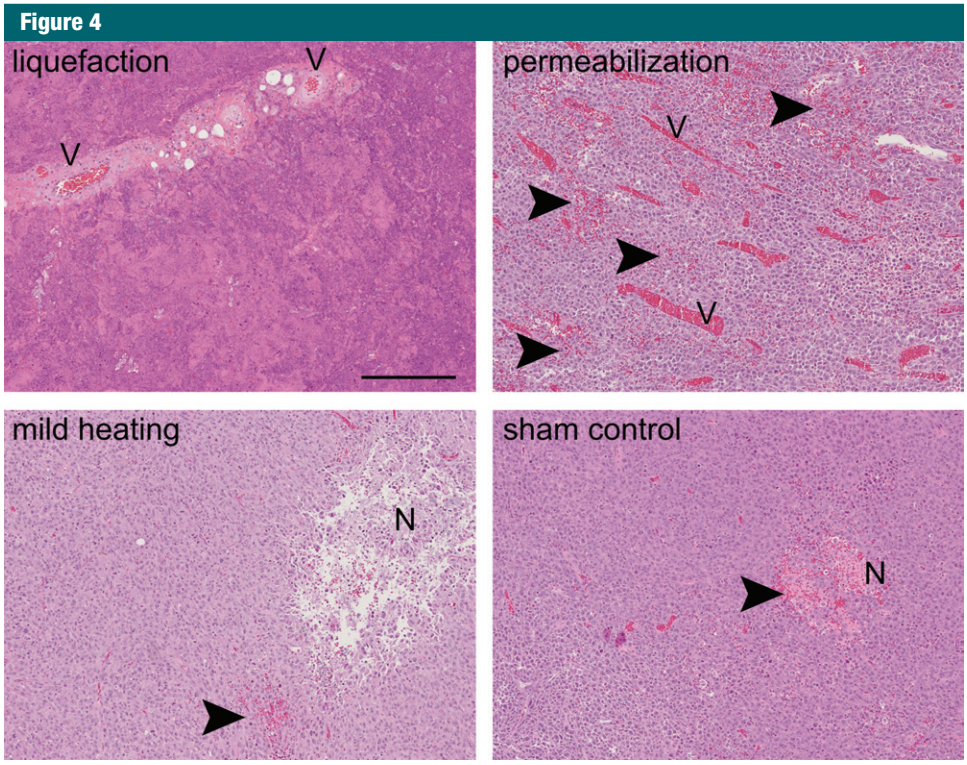

Figure 4: Histologic sections (hematoxylin-eosin stain; original magnification, ×10) of the tumors from the different treatment groups: liquefaction, permeabilization, mild heating, and sham control. Pockets of necrosis *(N)* and occasional areas of hemorrhage (arrowheads) were present in all tumors. Mild heating did not cause any noticeable histologic changes to tissue structure. The tissue liquefaction regimen resulted in complete disintegration of the tissue structure into subcellular debris, while sparing some of the connective tissue structures (eg, larger blood vessels *[V]*). The tissue permeabilization regimen caused areas of petechial hemorrhage (arrowheads). Scale bar is 250 microns.

region (that corresponded to the vapor bubble) appeared prefocally after each delivered pulse (Fig 3), which allowed monitoring of treatment progression in real time. The mild heating and tissue permeabilization regimes did not produce noticeable changes to the B-mode image of the tumor (Fig 3). Each spot received a 30-second treatment (for all treatments). The overall treatment time was 10–12 minutes (18–24 treatment points), depending on tumor size.

Immediately after focused ultrasound treatment, the animal was removed from the holder, and the first posttreatment blood withdrawal was performed (ie, at the 15-minute time point). After subsequent blood draws at 30 minutes and 1 hour, the animal was recovered from anesthesia and returned to its cage. The animal was briefly reanesthetized for two subsequent blood draws (ie, at 3-hour and 24-hour time points), followed by euthanasia. The tumor was then resected and fixed in 10% neutral buffered formalin, followed by processing and paraffin embedding for histologic analysis (J.R.C., T.D.K., Y.N.W., and G.R.S.; Fig 4).

To further characterize the dynamics of miRNA release, an additional cohort of grafted rats ($n = 7$) was treated with the tissue liquefaction regimen, and blood specimens were collected immediately prior to, during (2- and 8-minute time points), and within a short time after treatment (at 15-, 30-, and 45-minute time points). The animals were euthanized immediately after the last blood draw. The blood samples (approximately 0.5 mL) were immediately transferred to K2–edetic acid plasma tubes and homogenized via gentle inversion 20 times without shaking to avoid hemolysis. Tubes were then centrifuged for 15 minutes at 1300 times gravity (relative centrifugal force) at room temperature. Then, 250 μL of plasma was aspirated and immediately combined with 1.25 mL of Qiazol (Qiagen, Hilden, Germany), lysed as described previously (23), frozen on dry ice, and stored at −80°C until RNA extraction (J.R.C. and M.D.G., with 8 and 5 years of experience, respectively).

Types of Pulsed Focused Ultrasound Treatment

The acoustic parameter space for BH has been investigated previously, ex vivo and in vivo (21,24). Briefly, tissue liquefaction is achieved if the focal waveform contains a shock front with amplitude sufficient to induce vapor bubble formation (ie, boiling) in less than 20 msec, pulse lengths no more than two to four times longer than the time to reach boiling, and duty factors of less than 2%. In the present case,

Figure 5

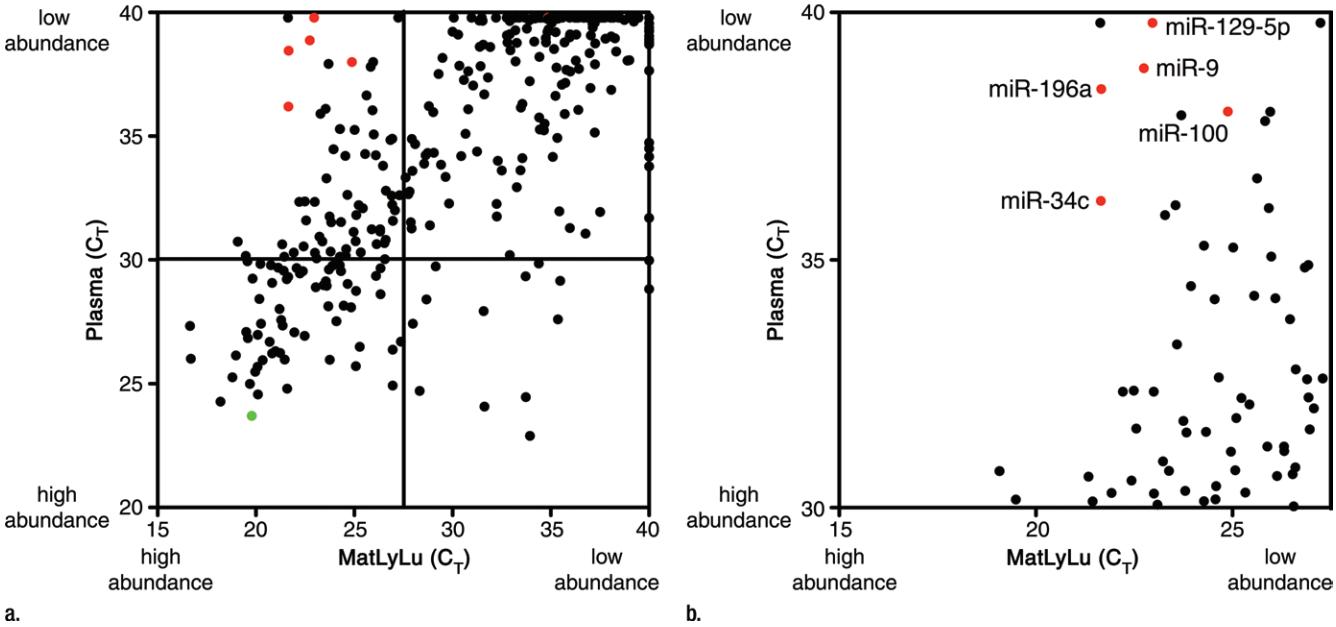

Figure 5: Scatterplots generated for the identification of candidate tumor biomarkers in the MatLyLu rat model system. miRNA expression profiling was performed by using RT-qPCR arrays to analyze RNA purified from the plasma of untreated control rats ($n = 4$) or from the MatLyLu tumor cell line. **(a)** miRNAs with higher abundance in the cell line (lower cycle threshold *[C_T]* values on the x-axis) and low or undetected abundance in untreated rat plasma (higher cycle threshold values on the y-axis) were selected as candidate biomarkers (shown in red). The nonbiomarker internal control miR-16 is shown in green. **(b)** Higher resolution image of the upper left quadrant of **a** can be used to identify candidate miRNAs. Candidate biomarkers are shown in red, and other miRNAs are shown in black.

the shock amplitude was 70 MPa (Fig 2b), and the time to reach boiling was estimated as 2.7 msec, according to weak shock theory. Therefore, pulse duration was chosen as 10 msec, and pulse repetition frequency was chosen as 1 Hz, which resulted in duty factor of 1%. The exposure duration at a single focal spot was chosen to be 30 seconds, which corresponded to the delivery of 30 pulses, after which the size of the lysed lesion reaches saturation (20). To keep the total treatment time similar between different types of exposures, the duration of the other two exposures was also defined as 30 seconds per focal spot.

Tissue permeabilization relies on inducing inertial cavitation in tissue at the focus by using pulsed exposures at a low duty factor to avoid thermal effects on tissue. The pulsed focused ultrasound exposure parameters used for tissue permeabilization were peak negative focal pressure of 16 MPa, pulse duration of 1 msec, and pulse repetition frequency of 1 Hz (18). To confirm consistent cavitation activity throughout exposure, broadband emissions that resulted from each focused ultrasound pulse were detected with a passive cavitation detector, and the signals were processed with a method similar to that in our previous studies to obtain the level of broadband noise emitted by cavitation bubbles (25). The details of passive cavitation detector signal acquisition, processing, and cavitation activity levels are given in Appendix E1 (online).

Mild heating of the tumor was achieved by using low-amplitude sonication, which was unlikely to cause cavitation, at a duty factor of 50% (2-msec pulse duration; pulse repetition frequency, 250 Hz). The temperature increase at the focus was estimated theoretically by using tissue thermal and acoustic parameters reported in the literature (26) after the cylindrical Gaussian beam approximation (27) to account for heat diffusion between focused ultrasound pulses. According to these calculations, the steady-state temperature increase at each focal spot was 9°C. Note that these estimates do not account for tissue perfusion.

miRNA Profiling and Identification of Candidate miRNA Biomarkers

RNA derived from four samples of untreated rat plasma and the MatLyLu cell line was used for discovery of candidate biomarkers (Fig 5). Samples were profiled for the relative abundance of 375 miRNAs by using miRNA ready-to-use polymerase chain reaction, human panel I, V2.M RT-qPCR arrays (Exiqon, Vedbaek, Denmark) (J.R.C., M.D.G.). Experimental details are presented in Appendix E1 (online).

Individual Real-Time Polymerase Chain Reaction Assays

TaqMan assays (Applied Biosystems, Foster City, Calif) for human miRNAs (identical to the rat sequences) *hsa*-miR-16, *hsa*-miR-34c, *hsa*-miR-100, *hsa*-miR-129–5p, and *hsa*-miR-196a, in

addition to *Caenorhabditis elegans* miRNA *cel*-miR-39, were obtained (Applied Biosystems). Oligoribonucleotides that corresponded to the mature sequence of each miRNA were synthesized (Integrated DNA Technologies, Coralville, Iowa) and serially diluted as standard curves (23). Individual miRNAs were detected with RT-qPCR, as described previously (28), with details presented in Appendix E1 (online) (J.R.C., with 8 years of experience).

Statistical Analysis

Tests and parameters are indicated in the corresponding Figure legends. All statistical analyses were performed by using Prism version 7.0a software (GraphPad Software, La Jolla, Calif) with criteria for significance given as *P* up to .05, *P* up to .01, or *P* up to .001 (J.R.C., T.D.K.).

Results

Histologic Tissue Changes after Focused Ultrasound Treatment

The structural alterations to tumor tissue by each type of focused ultrasound treatment were observed grossly (Fig E1 [online]) and confirmed at histologic evaluation (Fig 4). Tissue liquefaction through BH produced complete tissue disintegration into subcellular debris, with occasional intact nuclei observed in the lysate, but no other structurally intact cells or organelles. As is consistent with previous studies (16), this treatment appeared to be tissue selective: Some larger connective tissue structures in the treated region (eg, blood vessels) remained intact, while the tumor cells that surrounded the vessels were liquefied. Permeabilization treatment resulted in largely intact tumor tissue, with some damaged adjacent tumor cells and scattered areas of petechial hemorrhage. As expected, mild heating did not noticeably alter tissue structure.

Release of miRNA after Pulsed Focused Ultrasound Treatment

Liquefaction of the tumors significantly (*P* value range, .0006–.04) increased the plasma quantities of candidate miRNA biomarkers, with increases ranging from threefold to 32-fold for miR-34c, miR-100, miR-129–5p, and miR-196a within 15–30 minutes of the initiation of treatment, relative to pretreatment levels (Fig 6). The maximum plasma abundance for

Figure 6

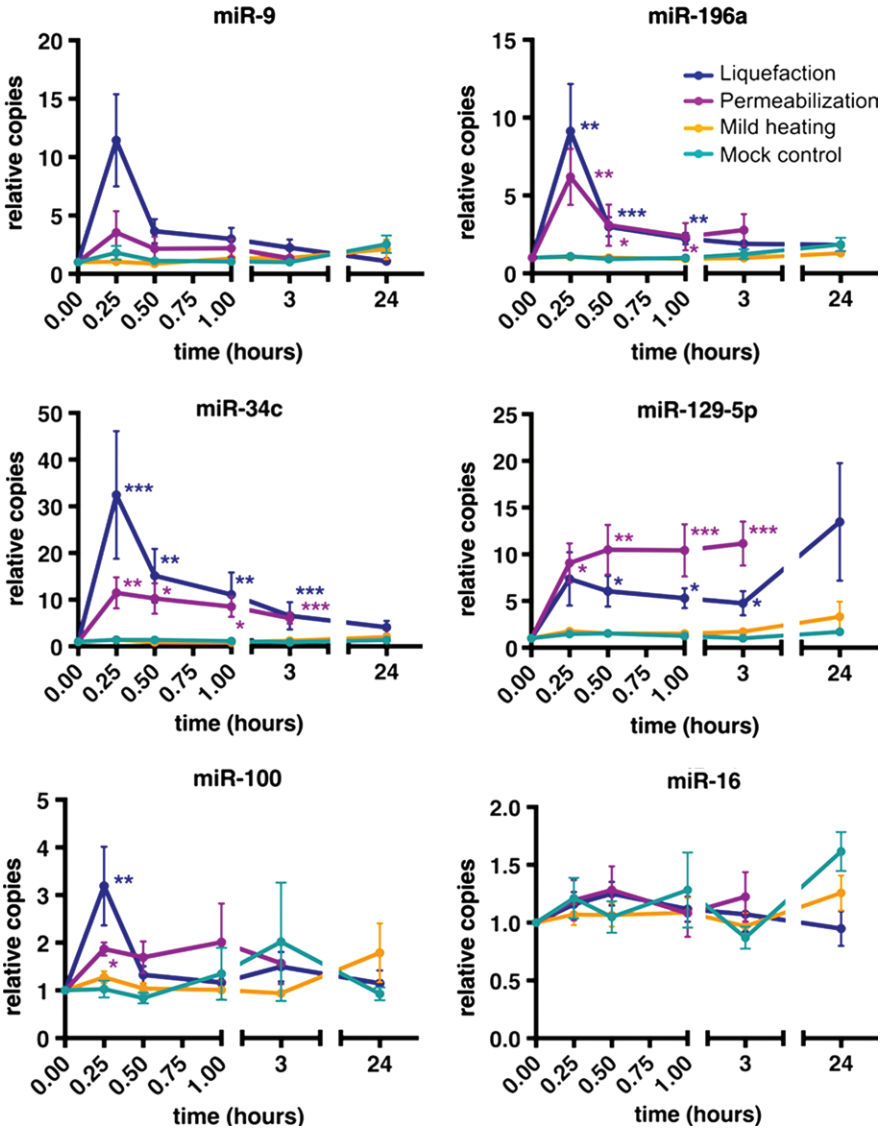

Figure 6: Graphs depict how pulsed focused ultrasound–induced liquefaction and permeabilization (but not mild heating) of tumors release tumor-specific miRNAs (miR-196a, miR-34c, miR-129–5p, and miR-100) into the blood circulation in vivo. Data are presented as means ± standard errors of the mean. Blood samples collected at the times indicated were processed into plasma immediately after collection, and RNA was extracted. Note that a time of 0 refers to pretreatment, and pulsed focused ultrasound treatment was performed during the first 15 minutes. miRNA was quantified by using RT-qPCR. Values on the y-axis are presented as copies relative to the pretreatment copies (ie, fold change). No significant increase in the abundance of the broadly expressed, miR-16–negative control miRNA (ie, not a tumor biomarker miRNA) is observed. *P* values are based on the comparison of treatment fold change values to mock treated control fold change values at each time point by using one-way analysis of variance (Kruskal-Wallis test), followed by the Dunn multiple-comparisons test. * = $P \leq .05$, ** = $P \leq .01$, *** = $P \leq .001$.

most miRNAs of interest (except miR-129–5p) was observed at 15 minutes, with levels returning to baseline over 30 minutes (miR-100), 3 hours (miR-196a), and 24 hours (miR-34c). Tissue permeabilization also increased the plasma abundance of most candidate miRNA biomarkers (with a smaller effect size of twofold to 11-fold), with a comparable kinetic trend. The mean abundance of miR-129–5p after tissue liquefaction remained increased 24 hours after treatment but was not statistically significant at this time point. Mild heating of the tumor yielded no significant ($P > .05$) increases among these miRNAs. miR-16, a circulating miRNA that serves as a systemic negative control (as its expression is not specific to the tumor and therefore is not a tumor biomarker), was not significantly ($P > .05$) increased by any treatment, which indicates that the treatment-dependent increase observed for the biomarker miRNAs was not the result of a proportional systemic, total increase in plasma miRNA abundance.

Further Characterization of miRNA Release Kinetics during Pulsed Focused Ultrasound–induced Liquefaction

RT-qPCR analysis of RNA isolated from the plasma samples collected during and within 45 minutes after tumor tissue liquefaction demonstrated significant (P = .01–.02) increases of miR-34c and miR-196a when compared with pretreatment levels within 2 minutes of initiating treatment (Fig 7). A significant increase (P = .005) was also detected for miR-100 within 8 minutes of treatment initiation. This time point corresponded to the production of four cylindrical liquefied voids, each with dimensions of approximately 2 × 7 mm (0.09-mL total volume), as estimated from B-mode US images. Rapid increase was also observed for miR-9, although without statistical significance in this cohort. Interestingly, candidate biomarker quantities did not increase substantially as the treatment progressed and larger tumor volume was liquefied. In agreement with previous results, effect sizes observed at 15 minutes approximated those observed in the separate experiments presented in Figure 6.

Figure 7

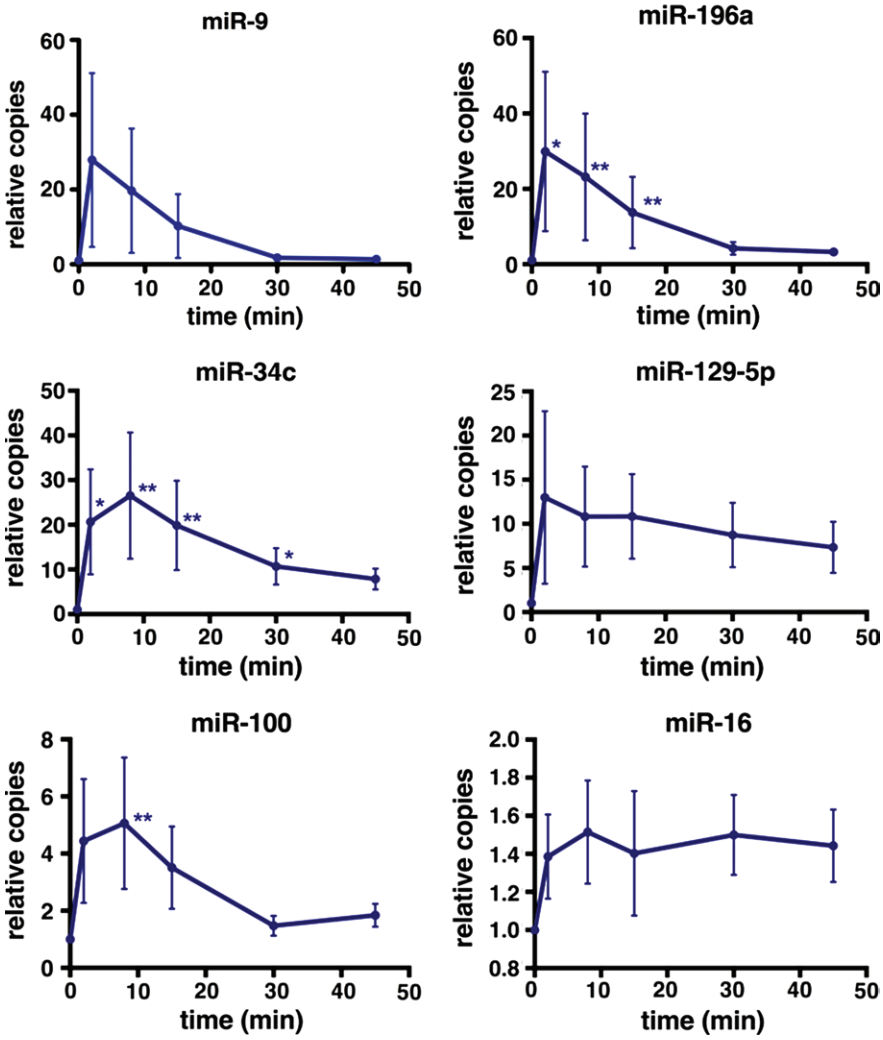

Figure 7: Graphs depict the dynamics of miRNA release during the first 15 minutes and immediately after (ie, 5–45 minutes after the initiation of treatment) tumor liquefaction with pulsed focused ultrasound. Data are presented as means ± standard errors of the mean. A significant increase in the abundance of miR-34c and miR-196a is observed within 2 minutes of treatment initiation and within 8 minutes for miR-100. *P* values for each treatment time point were calculated against the pretreatment miRNA abundance by using one-way analysis of variance (Friedman test), followed by the Dunn multiple-comparisons test. ∗ = $P \leq .05$, ∗∗ = $P \leq .01$.

Discussion

The use of circulating nucleic acid biomarkers as liquid biopsies for cancer diagnosis and treatment monitoring has been the subject of rapidly increasing research and is showing promise for clinical utility (10,11). However, the use of these biomarkers remains limited, as their origin cannot be identified and they are often present at or below quantifiable limits. We sought to overcome these challenges by using pulsed focused ultrasound as a method to stimulate the release of biomarkers from a precise anatomic location. Most anatomic locations would be accessible by using pulsed focused ultrasound, with exceptions for brain (due to the high attenuation of ultrasound in the skull),

bone, and lung. In a pioneer study, the application of low-intensity ultrasound was reported to significantly (P = .03) increase plasma CEA in tumor-bearing animals (14). Although cell-surface and secreted biomarkers like CEA can be useful, the ability to release intracellular biomarkers (especially nucleic acids) in vivo would have greater diagnostic utility and has not been explored previously.

We observed that pulsed focused ultrasound exposures that caused mechanical tissue disruption increased the abundance of candidate miRNA biomarkers in the plasma threefold to 32-fold in our rodent model. These increases almost immediately followed the initiation of pulsed focused ultrasound treatment, which suggests the direct release of miRNA from tumor cells with disrupted cellular membrane integrity into the circulation. The rapid rate of release and limited volume of disrupted tissue makes this approach logistically feasible for clinical application.

Although liquefaction of tumors by BH provided more miRNA release than cavitation-based tissue permeabilization, BH is more destructive and applicable to a relatively narrow set of clinical situations as a replacement for needle biopsy of a well-defined mass. In contrast, cavitation-based tissue permeabilization induces microscale tissue damage (ie, no more than would be expected to occur around biopsy needle cores). Therefore, this method would be suitable for a broader set of clinical applications that require minimal and possibly repeated sampling. Such applications may include serial tumor monitoring to assess response to treatment (eg, possible acquired resistance) and interrogating at-risk tissue in individuals with a high risk of cancer due to genetic predisposition. This would be especially suitable when the tumor mass is not well defined by the appropriate imaging modality.

Standardization of pulsed focused ultrasound exposures to induce repeatable disruption of the tissue of interest is an important requirement to enable clinical implementation. In the case of BH, the size of the liquefied region presents a standardization metric that can be monitored in real time (21). Cavitation activity that induces tissue permeabilization can be quantified via passive cavitation detector, and the derived metrics have been demonstrated to correlate with the resulting microscale tissue damage (18). However, this approach does not provide the spatial distribution of cavitation bubbles in tissue. Two US-based techniques have emerged that allow imaging of pulsed focused ultrasound–induced bubbles, thus providing a means to monitor and standardize these exposures (29,30).

The influence of pulsed focused ultrasound on the risk of tumor dissemination has long been a subject of debate (31,32). One hypothesis of concern is the release of viable tumor cells into circulation and possible metastasis. However, our current understanding of the metastatic process requires cancer cells to acquire mutations that promote survival in the circulation and colonization of distant organs (33), not merely mechanical disruption and displacement of tumor cells. In addition, pulsed focused ultrasound–induced alterations are confined to the targeted area, unlike the disruption of intervening tissues with needle biopsy. Thus, it may be even less likely to cause tumor dissemination. Independently, pulsed focused ultrasound treatment may alter the cytokine milieu, which may enable or suppress metastasis. In one preclinical study, investigators reported that histotripsy and cavitation-based therapies suppress tumor growth and formation of metastases through stimulation of antitumor immune response (31). However, rigorous and specific preclinical studies are required (and are currently underway) to determine the safety of this approach.

Multiple limitations of our study provide motivation for future experiments: First, it is worth considering the anatomic and physiological differences between our rat model system and human patients. Rats have substantially less blood volume, a relatively larger tumor size (due to the grafted tumors), and a higher heart rate than humans. We hypothesize that the kinetics of biomarker release are unlikely to be substantially different between species, as this appears to occur within minutes after pulsed focused ultrasound exposure, and the influence of the twofold difference in heart rate is expected to be minor. In contrast, the magnitude of the effect is more likely to be affected by the differences in total blood volume and the pulsed focused ultrasound-treated tissue volume. In addition, the rate of background release is also likely to be tumor dependent, which indicates that once optimized for maximum yield with minimal tissue damage in the small animal model, the pulsed focused ultrasound approach will require testing in larger species and other types of tumors along the pathway to clinical development. Furthermore, in our study, we examined only one class of circulating nucleic acid biomarkers (miRNAs), which have been shown to be highly stable in plasma and can be robustly measured. It serves as the proof-of-concept for an approach that could be applied to enhance blood-based detection of other types of cancer biomarkers as well, including cell-free circulating tumor DNA, thus amplifying the potential clinical applications of this approach.

In conclusion, pulsed focused ultrasound offers a unique capability to produce localized, controlled mechanical disruption of tissue noninvasively and provides a method to stimulate the release of intracellular biomarkers into the circulation, where their increased quantities can be accessed more readily and used to guide patient care.

Acknowledgment: The art for Figure 1 was prepared by Mesa Schumacher, Information Art and Design.

Disclosures of Conflicts of Interest: J.R.C. Activities related to the present article: disclosed no relevant relationships. Activities not related to the present article: author is an employee of RainDance Technologies. Other relationships: author has a patent pending for high-intensity focused ultrasound. **T.D.K.** Activities related to the present article: disclosed no relevant relationships. Activities not related to the present article: disclosed no relevant relationships. Other relationships: author has patents pending for high-intensity focused ultrasound and imaging bubbles in a medium. **M.D.G.** disclosed no relevant relationships. **G.R.S.** Activities related to the present article: disclosed no relevant relationships. Activities not related to the present article: disclosed no relevant relationships. Other relationships: author has a patent pending (61/974,317). **F.S.** disclosed

no relevant relationships. **Y.N.W.** disclosed no relevant relationships. **E.N.G.** disclosed no relevant relationships. **K.W.** disclosed no relevant relationships. **J.H.H.** Activities related to the present article: disclosed no relevant relationships. Activities not related to the present article: disclosed no relevant relationships. Other relationships: author has patents pending for high-intensity focused ultrasound and imaging bubbles in a medium. **M.T.** Activities related to the present article: disclosed no relevant relationships. Activities not related to the present article: author received payment from Miroculus and CustomArray for consulting. Other relationships: author has a patent pending for high-intensity focused ultrasound.

References

1. Roychowdhury S, Iyer MK, Robinson DR, et al. Personalized oncology through integrative high-throughput sequencing: a pilot study. Sci Transl Med 2011;3(111):111ra121.
2. Mirnezami R, Nicholson J, Darzi A. Preparing for precision medicine. N Engl J Med 2012; 366(6):489–491.
3. Borboroglu PG, Comer SW, Riffenburgh RH, Amling CL. Extensive repeat transrectal ultrasound guided prostate biopsy in patients with previous benign sextant biopsies. J Urol 2000;163(1):158–162.
4. Wolters T, van der Kwast TH, Vissers CJ, et al. False-negative prostate needle biopsies: frequency, histopathologic features, and follow-up. Am J Surg Pathol 2010;34(1):35–43.
5. Yuen JS, Lau WK, Ng LG, Tan PH, Khin LW, Cheng CW. Clinical, biochemical and pathological features of initial and repeat transrectal ultrasonography prostate biopsy positive patients. Int J Urol 2004;11(4):225–231.
6. Djavan B, Waldert M, Zlotta A, et al. Safety and morbidity of first and repeat transrectal ultrasound guided prostate needle biopsies: results of a prospective European prostate cancer detection study. J Urol 2001;166(3): 856–860.
7. Saad A, Hanbury DC, McNicholas TA, Boustead GB. Acute periprostatic haematoma following a transrectal ultrasound-guided needle biopsy of the prostate. Prostate Cancer Prostatic Dis 2002;5(1):63–64.
8. Aly M, Dyrdak R, Nordström T, et al. Rapid increase in multidrug-resistant enteric bacilli blood stream infection after prostate biopsy—a 10-year population-based cohort study. Prostate 2015;75(9):947–956.
9. Mitchell PS, Parkin RK, Kroh EM, et al. Circulating microRNAs as stable blood-based markers for cancer detection. Proc Natl Acad Sci U S A 2008;105(30):10513–10518.
10. Diehl F, Li M, Dressman D, et al. Detection and quantification of mutations in the plasma of patients with colorectal tumors. Proc Natl Acad Sci U S A 2005;102(45):16368–16373.
11. Leary RJ, Kinde I, Diehl F, et al. Development of personalized tumor biomarkers using massively parallel sequencing. Sci Transl Med 2010;2(20):20ra14.
12. Hindson CM, Chevillet JR, Briggs HA, et al. Absolute quantification by droplet digital PCR versus analog real-time PCR. Nat Methods 2013;10(10):1003–1005.
13. Witwer KW. Circulating microRNA biomarker studies: pitfalls and potential solutions. Clin Chem 2015;61(1):56–63.
14. D'Souza AL, Tseng JR, Pauly KB, et al. A strategy for blood biomarker amplification and localization using ultrasound. Proc Natl Acad Sci U S A 2009;106(40):17152–17157.
15. Kopechek JA, Kim H, McPherson DD, Holland CK. Calibration of the 1-MHz Sonitron ultrasound system. Ultrasound Med Biol 2010;36(10):1762–1766.
16. Khokhlova VA, Fowlkes JB, Roberts WW, et al. Histotripsy methods in mechanical disintegration of tissue: towards clinical applications. Int J Hyperthermia 2015;31(2):145–162.
17. Martin KH, Dayton PA. Current status and prospects for microbubbles in ultrasound theranostics. Wiley Interdiscip Rev Nanomed Nanobiotechnol 2013;5(4):329–345.
18. Li T, Wang YN, Khokhlova TD, et al. Pulsed high-intensity focused ultrasound enhances delivery of doxorubicin in a preclinical model of pancreatic cancer. Cancer Res 2015; 75(18):3738–3746.
19. Miao CH, Brayman AA, Loeb KR, et al. Ultrasound enhances gene delivery of human factor IX plasmid. Hum Gene Ther 2005;16(7):893–905.
20. Khokhlova TD, Canney MS, Khokhlova VA, Sapozhnikov OA, Crum LA, Bailey MR. Controlled tissue emulsification produced by high intensity focused ultrasound shock waves and millisecond boiling. J Acoust Soc Am 2011;130(5):3498–3510.
21. Khokhlova TD, Wang YN, Simon JC, et al. Ultrasound-guided tissue fractionation by high intensity focused ultrasound in an in vivo porcine liver model. Proc Natl Acad Sci U S A 2014;111(22):8161–8166.
22. Isaacs JT, Yu GW, Coffey DS. The characterization of a newly identified, highly metastatic variety of Dunning R 3327 rat prostatic adenocarcinoma system: the MAT LyLu tumor. Invest Urol 1981;19(1):20–23.
23. Chevillet JR, Kang Q, Ruf IK, et al. Quantitative and stoichiometric analysis of the microRNA content of exosomes. Proc Natl Acad Sci U S A 2014;111(41):14888–14893.
24. Canney MS, Khokhlova VA, Bessonova OV, Bailey MR, Crum LA. Shock-induced heating and millisecond boiling in gels and tissue due to high intensity focused ultrasound. Ultrasound Med Biol 2010;36(2):250–267.
25. Li T, Chen H, Khokhlova T, et al. Passive cavitation detection during pulsed HIFU exposures of ex vivo tissues and in vivo mouse pancreatic tumors. Ultrasound Med Biol 2014; 40(7):1523–1534.
26. Duck FA. Physical properties of tissue: a comprehensive reference book. London, England: Academic Press, 1990.
27. Parker KJ. The thermal pulse decay technique for measuring ultrasonic-absorption coefficients. J Acoust Soc Am 1983;74(5):1356–1361.
28. Kroh EM, Parkin RK, Mitchell PS, Tewari M. Analysis of circulating microRNA biomarkers in plasma and serum using quantitative reverse transcription-PCR (qRT-PCR). Methods 2010;50(4):298–301.
29. Li T, Khokhlova TD, Sapozhnikov OA, O'Donnell M, Hwang JH. A new active cavitation mapping technique for pulsed HIFU applications—bubble Doppler. IEEE Trans Ultrason Ferroelectr Freq Control 2014;61(10): 1698–1708.
30. Jensen CR, Ritchie RW, Gyöngy M, Collin JR, Leslie T, Coussios CC. Spatiotemporal monitoring of high-intensity focused ultrasound therapy with passive acoustic mapping. Radiology 2012;262(1):252–261.
31. Xing Y, Lu X, Pua EC, Zhong P. The effect of high intensity focused ultrasound treatment on metastases in a murine melanoma model. Biochem Biophys Res Commun 2008; 375(4):645–650.
32. Oosterhof GO, Cornel EB, Smits GA, Debruyne FM, Schalken JA. The influence of high-energy shock waves on the development of metastases. Ultrasound Med Biol 1996; 22(3):339–344.
33. Hanahan D, Weinberg RA. The hallmarks of cancer. Cell 2000;100(1):57–70.